Physica A 466 (2017) 552–569

Contents lists available at ScienceDirect

Physica A

journal homepage: www.elsevier.com/locate/physa

Effects of a periodic drive and correlated noise on birhythmic van der Pol systems

R. Mbakob Yonkeu [a], R. Yamapi [b,*], G. Filatrella [c], C. Tchawoua [a]

[a] Laboratory of Mechanics and Materials, Department of Physics, Faculty of Science, University of Yaoundé I, Box 812, Yaoundé, Cameroon
[b] Fundamental Physics Laboratory, Department of Physics, Faculty of Science, University of Douala, Box 24 157 Douala, Cameroon
[c] Department of Sciences and Technologies and Salerno unit of CNSIM, University of Sannio, Via Port'Arsa 11, I-82100 Benevento, Italy

HIGHLIGHTS

- A forced, stochastic van der Pol type birhythmic oscillator is considered.
- The noise is correlated.
- The analytical treatment allows the reduction to a bistable pseudopotential.
- Numerical simulations confirm the effectiveness of the stochastic averaging.
- The interplay of the drive and noise produces structural changes.

ARTICLE INFO

Article history:
Received 10 April 2016
Received in revised form 5 July 2016
Available online 23 September 2016

Keywords:
Correlation time
Deterministic force
Birhythmic system
Residence time
Bifurcation

ABSTRACT

This paper considers the dynamics of a van der Pol birhythmic oscillator submitted both to colored noise and harmonic excitation. Applying the quasi-harmonic assumption to the corresponding Langevin equation we derive an approximated Fokker–Planck equation, that is compared with the results of computer simulations. We thus derive both the effects of the correlation time and the harmonic excitation on the parameter space where birhythmicity appears. In this region, we find that the multi-limit-cycle van der Pol oscillator reduces to an asymmetric bistable system where the sinusoidal drive intensity plays the role of asymmetric parameter, and noise can lead to stochastic bifurcations, consisting in a qualitative change of the stationary amplitude distribution. Under both influence of noise and harmonic excitation, the dynamics can be well characterized through the concepts of pseudo-potential, that regulates the low noise Arrhenius-like behavior.

1. Introduction

Many problems in physics, chemistry, or biology are related to the behavior of nonlinear self-excited oscillators [1]. In particular, we are here interested in birhythmic systems [2–16], i.e. in the possibility that a system exhibits two limits cycles of different amplitude and frequency, and consequently a bistable behavior: the displayed limit cycle depends upon the initial conditions. To this underlying deterministic dynamics, noise, inevitable in real process, can have profound consequences, for the stability of dynamical systems can be strongly affected by the presence of uncontrolled perturbations [17]. For instance, noise can induce a shift of the bifurcations to different control values, or a qualitative

* Corresponding author.
E-mail address: ryamapi@yahoo.fr (R. Yamapi).

http://dx.doi.org/10.1016/j.physa.2016.09.012
0378-4371/

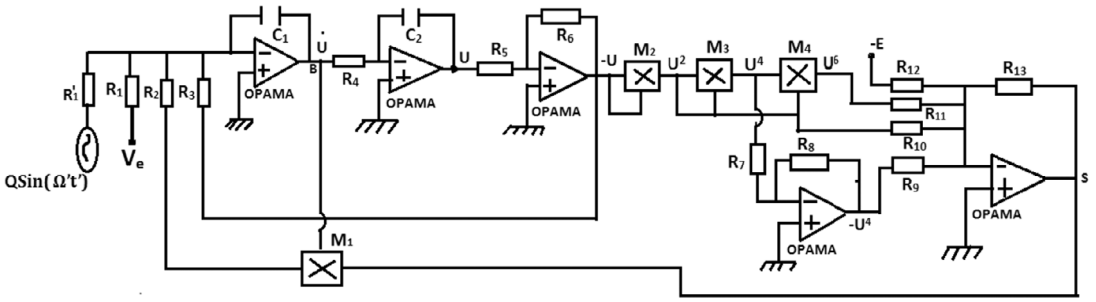

Fig. 1. Circuit diagram for an electronic circuit that approximately describes a birhythmic van der Pol type, Eq. (4). Here the M_i are analog multipliers circuits, while the operation amplifiers with feedback capacitors perform analog integrations.

change of the stationary probability density function [18]. The presence of a periodic signal can possibly induce the transition from one metastable state to another and noise can induce even an enhancement of the response to a periodic drive as in stochastic resonance [19], although the interpretation in signal processing should be taken with some care [20]. Noise induced bifurcation is of primary interest for instance in electronic circuits [21], mechanical oscillators [22] and laser physics [17]. As stochastic analysis of physical problems has broadened, the need for more realism in models has grown, and the correlation time of the noise driving the stochastic process has attracted much attention [23]. In particular, the presence of exponential correlations [24] described by the Ornstein–Uhlenbeck process can be taken into account by adding an extra dimension to the dynamical system [25]. We consider, to be specific, van der Pol oscillators, that occur in a large number of applications such as signal detection [26], electrical circuits, the beating of a heart, and sound acoustics [27].

We further focus on a special version of the van der Pol oscillator found in biological systems [2,3]. *The noiseless case was first considered to characterize the attractors with different frequencies* [4,6], *also coupled* [28]. *Uncorrelated noise and delayed feedback were included* [9,10], *and the noisy system has been investigated with the use of the quasipotential* [11,12,16]. *van der Pol birhythmic oscillators might be considered a protypal system for birhythmic behavior observed especially, but not only, in biological systems* [5,7,8,13–15]. The presented model is also derived from an electrical circuit equivalent of the modified van der Pol system [29]. We do so on the practical side to indicate a practical realization that might be used to verify the analytic and numerical predictions. On the more abstract side, we find it convenient to indicate a practical model that neglects the complications connected with biological models of the van der Pol type, but that are of course only approximated by the present model. We feel that this is particularly necessary in this context of forced oscillations [15], for external drives are less obviously applicable to biochemical systems.

This paper is structured as follows: Section 2 gives the dynamic features of the forced birhythmic van der Pol oscillator. *Sections 2.2 and 2.3 report the case of undriven oscillations as in Ref.* [16], *and therefore are only reported here to make the work self consistent. Instead, Section 2.4, although similar in the approach to the case of non-forced oscillations, contains the original calculations that lead to the main results of this work, the pseudopotential (19) and (20) and the Fokker–Planck equation (22). In fact* Section 3 describes the pseudo-potential and energy barriers for the periodic attractors. In Section 4, the Fokker–Planck equation of the averaged orbit probability distribution is studied. Section 5 shows the algorithm for colored noise and numerical results. Section 6 concludes this work.

2. Dynamic features of the forced birhythmic van der Pol oscillator

In this section we present a version of van der Pol model (henceforth: BvdP) that we use as a prototype of birhythmic systems. We do so also introducing the electrical equivalent circuit, and the normalized equations are derived.

2.1. Circuit description and model equations

The model used in our analysis can be reproduced with electronic circuits. An example of equivalent circuit is shown in Fig. 1. It consists of electronic multipliers M_i ($i = 1, \ldots, 4$), integrators, that are operational amplifiers with a feedback capacitor, and sommators, realized by operational amplifiers with multiple input resistors (this electronics circuit without sinusoidal signal has already been studied in Ref. [16]). Using Millman law, the characteristics of each component, the contributions of the electrical voltage V_e, (that in this study is assumed to be a random term) and a sinusoidal voltage supplied by an external source, we find for the potential at the left of the point S:

$$V_s = E\frac{R_{13}}{R_{12}} - \frac{R_{13}}{R_{10}}\frac{V^2}{K} + \frac{R_{13}}{R_9}\frac{V^4}{K^3} - \frac{R_{13}}{R_{11}}\frac{V^6}{K^5}, \tag{1}$$

where K is a scaling factor, which has the dimension of a voltage. The multiplicator M_1 gives the end voltage (the dots denote the time derivative):

$$\int \left(\frac{V_e}{R_1C_1} + \frac{Q}{R_1'C_1}\sin(\Omega t) - \frac{V}{R_3C_1} + \frac{V_s}{K}\dot{V}\right)\frac{dt'}{R_2C_1} = \dot{V}. \tag{2}$$

Taking the time derivative of Eq. (2), one gets:

$$R_2C_1\ddot{V} - \frac{E}{K}\frac{R_{13}}{R_{12}}\left(1 - \frac{R_{12}}{R_{10}E}\frac{V^2}{K} + \frac{R_12}{R_9E}\frac{V^4}{K^3} - \frac{R_{12}}{R_{11}E}\frac{V^6}{K^5}\right)\dot{V} + \frac{1}{R_3C_1}V = \frac{V_e}{R_1C_1} + \frac{Q}{R_1'C_1}\sin(\Omega' t'). \tag{3}$$

It is convenient to introduce the variables $t = \omega_0 t'$ and $V = V_0 x$ where V_0 is the reference voltage and $\omega_0^2 = 1/\left(R_2R_3C_1^2\right)$ is the frequency. With the constraint $R_{12}V_0^2 = R_{10}EK$, Eq. (3) becomes the following non-dimensional differential equation:

$$\ddot{x} - \mu(1 - x^2 + \alpha x^4 - \beta x^6)\dot{x} + x = \eta(t) + \Xi_0 \sin(\Omega t) \tag{4}$$

where

$$\alpha = \frac{R_{12}V_0^4}{R_9EK^3}; \qquad \beta = \frac{R_{12}V_0^6}{R_{11}EK^5}; \qquad \mu = \frac{R_{13}E}{KR_2C_1R_{12}\omega_0};$$
$$\Omega = \frac{\Omega'}{\omega_0}; \qquad \eta = \frac{R_3}{R_1V_0}V_e; \qquad \Xi_0 = \frac{R_3}{R_1'V_0}Q.$$

Thus, in Eq. (4) the left hand side is the normalized equation of the birhythmic van der Pol system $x(t)$, and the deterministic force is characterized by an amplitude Ξ_0 and a frequency Ω. At the right hand side there is the correlated noise $\eta(t)$. The behavior of the system is not deterministic, for the evolution of $x(t)$ is subjected to the influence of random fluctuations. The BvdP system is governed by the parameters α and β (that in the biochemical system measure the degree of tendency of the system to a ferroelectric instability), and the strength of the nonlinear damping μ (see Ref. [9] for details).

2.2. Features of the exponentially correlated Gaussian noise

An important colored noise model often used in theoretical analysis and analogical experiments is the exponentially correlated noise [30], reproduced by the Langevin equation:

$$\dot{\eta}(t) = -\frac{1}{\tau}\eta(t) + \frac{\sqrt{2D}}{\tau}g_w(t). \tag{5}$$

Here, τ and D denote the correlation time and intensity of the colored noise, respectively, and $g_w(t)$ is a Gaussian variable with average 0 and standard deviation 1.

Eq. (5) is in this context employed just for numerical and analytical convenience, as we assume the noise to be correlated on the basis of the physical necessity (as in Ref. [31]) to correctly describe some systems. A reverse procedure can be used for multi-dimensional problems that are reduced to a lower dimensional problem at the price of the nonMarkovian character of the noise [32,33]. The particular form of the equation describing the evolution of $\eta(t)$ guarantees that the noise correlation exhibits a colored noise with exponential decay characterized by a correlation time τ:

$$\langle\eta(\tilde{t})\rangle = 0, \tag{6a}$$

$$\{\langle\eta(t), \eta(\tilde{t})\rangle\} = \frac{D}{\tau}\exp\left(-\frac{|t - \tilde{t}|}{\tau}\right). \tag{6b}$$

Here $\langle\cdot\rangle$ denotes averaging with respect to realizations and $\{\cdot\}$ denotes the averaging over the distribution of initial values of η. As the process is stationary, the distribution of the initial values of η is equal to the steady-state distribution, that is

$$P(\eta) = \sqrt{2\pi\frac{D}{\tau}}\exp\left(-\frac{\eta^2\tau}{2D}\right). \tag{7}$$

2.3. Approximated analysis of the undriven system

We consider in this subsection the case where the model is not influenced by an external noise excitation ($D = 0$) and without a deterministic force ($\Xi_0 = 0$), i.e. a nonlinear self-sustained oscillator which possesses more than one stable limit-cycle solution [4,34,9]. The amplitudes A_i and the frequencies Ω_i ($i = 1, 2, 3$) of the limit cycle solutions have been established in Refs. [34,9] starting from the approximated solution:

$$x(t) = A\cos(\Omega t). \tag{8}$$

Using the Lindsted perturbation method [35], one obtains that the amplitude A is independent of the coefficient μ up to correction of the order μ^2 and implicitly given by the relation

$$1 - \frac{1}{4}A^2 + \alpha\frac{1}{8}A^4 - \frac{5\beta}{64}A^6 = 0. \tag{9}$$

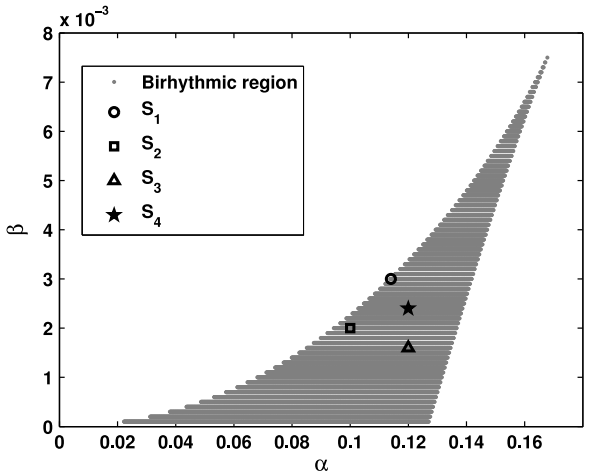

Fig. 2. Parameter region of the single limit cycle (white area) and three limit cycles (gray area) with $\mu = 0.01$ as obtained from simulations of Eq. (4) without noise ($\eta(t) = 0$) and no drive ($\Xi_0 = 0$). The symbols refer to the parameter sets investigated in this work, see Table 1.

Table 1
Characteristics of the limit cycles when the two frequencies are about equal (*i.e.* $\Omega_1 \simeq \Omega_3$, S_1 and S_2) and when the two frequencies are markedly different (*i.e.* $\Omega_1 \neq \Omega_3$, S_3 and S_4), as per Eq. (10). All data refer to the case $\mu = 0.01$.

$S_i = (\alpha, \beta)$	Amplitudes A_i of the orbits	Frequencies Ω_i of the orbits	Periods T_i of the orbits
$S_1 = (0.114; 0.003)$	$A_1 = 2.37720$ $A_2 = 5.02638$ $A_3 = 5.46665$	$\Omega_1 = 1.00212$ $\Omega_2 = 1.00113$ $\Omega_3 = 1.0231$	$T_1 = 6.270$ $T_2 = 6.275$ $T_3 = 6.141$
$S_2 = (0.1; 0.002)$	$A_1 = 2.3069$ $A_2 = 4.8472$ $A_3 = 7.1541$	$\Omega_1 = 0.98700$ $\Omega_2 = 1.000113$ $\Omega_3 = 0.971230$	$T_1 = 6.366$ $T_2 = 6.275$ $T_3 = 6.468$
$S_3 = (0.12; 0.0016)$	$A_1 = 2.481848$ $A_2 = 3.586374$ $A_3 = 10.048778$	$\Omega_1 = 1.00034$ $\Omega_2 = 0.999929058$ $\Omega_3 = 0.729350$	$T_1 = 6.2809$ $T_2 = 6.2845$ $T_3 = 9.2352$
$S_4 = (0.12; 0.0024)$	$A_1 = 2.448359$ $A_2 = 3.886565$ $A_3 = 7.6746428$	$\Omega_1 = 0.9892961$ $\Omega_2 = 0.99988893$ $\Omega_3 = 0.8670330$	$T_1 = 6.3510$ $T_2 = 6.2837$ $T_3 = 7.2466$

In the deterministic limit, the oscillator has fixed points (orbits) that depend on the values of the parameters (α, β), as there are up to three roots A_1, A_2, A_3 of Eq. (9), the inner stable orbit, the middle unstable orbit, and the outer stable orbit, respectively. In Fig. 2 we show the region (gray) of birhythmicity in the two parameters domain (α, β), where three attractors coexist, albeit only two of them are stable [4]. While the amplitude A is independent of the coefficient μ, see Eq. (9), the frequencies Ω_i $(i = 1, 2, 3)$ are not, for they are implicitly given by the relation:

$$\Omega_i = 1 - \mu^2 \frac{3}{64} A_i^2 + \mu^2 \left(\frac{1}{128} + \mu^2 \frac{\alpha}{24} \right) A_i^4 - \mu^2 \left(\frac{73\beta}{2048} + \mu^2 \frac{\alpha}{96} \right) A_i^6 + \mu^2 \left(\frac{67\beta}{8192} + \mu^2 \frac{3\alpha^2}{1024} \right) A_i^8 - \mu^2 \frac{69\alpha\beta}{16384} A_i^{10} + \mu^2 \frac{93\beta^2}{65536} A_i^{12} + 0(\mu^2). \tag{10}$$

The parameter sets $S_i(\alpha, \beta)$ used in this work are shown in Table 1, where the amplitude A_i, the frequency Ω_i and periods T_i for each parameter set are reported.

2.4. Analysis of forced oscillations

Here, we consider the forced BvdP oscillator governed by Eq. (4), without noise ($\eta(t) = 0$). Assuming that the fundamental component of the solution and the external excitation have the some period, the amplitude of the oscillations can be tackled using the harmonic balance method [36]. We consequently assume the solution is of the form (we recall that Ω is the frequency of the driving sinusoidal term):

$$x = A \sin(\Omega t) + \xi. \tag{11}$$

Here, as before in Eq. (8), A represents the amplitude of the oscillations, while $\xi \ll 1$ is a new constant. Inserting Eq. (11) in Eq. (4) without noise, one obtains

$$p_1 \sin(\omega t) + \xi + p_2 \cos(\Omega t) + p_3 \sin(2\Omega t) + p_4 \cos(3\Omega t) + p_5 \sin(4\Omega t) + p_6 \cos(5\Omega t) + p_7 \sin(6\Omega t) + p_8 \cos(7\Omega t) = \Xi_0 \sin(\Omega t) \tag{12}$$

with

$$\begin{aligned}
p_1 &= A - A\Omega^2,\\
p_2 &= -\mu\Omega A + \frac{\mu\Omega}{4}A^3 - \frac{\mu\alpha\Omega}{8}A^5 + \frac{5\mu\beta\Omega}{64}A^7 - \frac{3\mu\Omega\alpha\xi^2}{2}A^3 + \frac{15\mu\Omega\beta\xi^2}{8}A^5 + \frac{15\mu\Omega\beta\xi^4}{4}A^3 - \mu\Omega\alpha\xi^4 A + \mu\Omega\beta\xi^6 A + \Omega\xi^2 A,\\
p_3 &= -\mu\Omega\alpha\xi A^4 + \frac{15\mu\Omega\beta\xi}{16}A^6 + 5\mu\Omega\beta\xi^3 A^4 - 2\mu\Omega\alpha\xi^3 A^2 + 3\mu\Omega\beta\xi^5 A^2 + \mu\Omega\xi A^2\\
p_4 &= -\frac{\mu\omega}{4}A^3 + \frac{3\mu\alpha\Omega}{16}A^5 - \frac{9\mu\Omega\alpha}{64}A^7 + \frac{3\mu\alpha\Omega\xi^2}{2}A^3 - \frac{45\mu\Omega\beta\xi^2}{16}A^5 - \frac{15\mu\Omega\beta\xi^4}{4}A^3,\\
p_5 &= \frac{\mu\Omega\alpha\xi}{2}A^4 - \frac{3\mu\Omega\beta\xi}{4}A^6 - \frac{5\mu\Omega\beta\xi^3}{2}A^2,\\
p_6 &= -\frac{\mu\Omega\alpha}{16}A^5 + \frac{5\mu\Omega\beta}{64}A^7 + \frac{15\mu\Omega\beta\xi^2}{16}A^5,\\
p_7 &= \frac{3\mu\Omega\beta\xi}{16}A^6,\\
p_8 &= -\frac{\mu\Omega\beta}{64}A^7.
\end{aligned}$$

Equating the constants and the coefficients of $\sin(\Omega t)$ and $\cos(\Omega t)$ one has:

$$\begin{cases} p_1 = \Xi_0,\\ \xi = 0,\\ p_2 = 0, \end{cases} \tag{13}$$

that in turn implies:

$$\begin{cases} A\left(1-\Omega^2\right) = \Xi_0,\\ \mu\Omega A\left(1 - \frac{1}{4}A^2 + \frac{\alpha}{8}A^4 - \frac{5\beta}{64}A^6\right) = 0. \end{cases} \tag{14}$$

From the first of Eq. (14) one gets the amplitude:

$$A = \frac{\Xi_0}{(1-\Omega^2)}. \tag{15}$$

Fig. 3 displays the amplitude of the limit cycles A vs frequency Ω (up to the limit value $\Omega = 1$ that represents the frequency of the linear oscillations) of the deterministic force for different values of drive amplitude Ξ_0. When the intensity Ξ_0 of the deterministic drive increases, this limit value of A decreases, and we do not find solutions for the frequency $\Omega = 1$.

3. Pseudo-potential and energy barriers for the periodic attractors

This section deals with an analytical investigation of the pseudo-potential [37–39] associated to the equation of the self-sustained system Eq. (4). The pseudo-potential or quasipotential governs the low noise limit behavior of a system, even if it does not possess a *bona fide* potential. Moreover, the pseudopotential indicates the presence of metastable states, and it can be therefore used to characterize the metastable limit cycles of the birhythmic system. If, due to a change of parameters, the number of (pseudo) potential wells changes, one can also assert that a transition between unimodal to bimodal (and vice versa) distribution has occurred. The transitions between the unimodal and the bimodal stationary densities are also referred to as the noise induced transition or stochastic bifurcation.

To retrieve the pseudopotential, we assume the oscillations at a frequency close to the natural frequency, $w = \Omega + \nu$, with $\nu \ll 1$. To treat the effects of noise, we use the Krylov–Bogoliubov averaging method [40,41] to find the instantaneous amplitude and the associated pseudo-potential. In the quasiharmonic regime, assuming that the noise intensity is small and using the change of variables:

$$\begin{aligned} x(t) &= A(t)\cos(wt + \varphi(t)),\\ u(t) &= \dot{x}(t) = -wA(t)\sin(wt + \varphi(t)), \end{aligned} \tag{16}$$

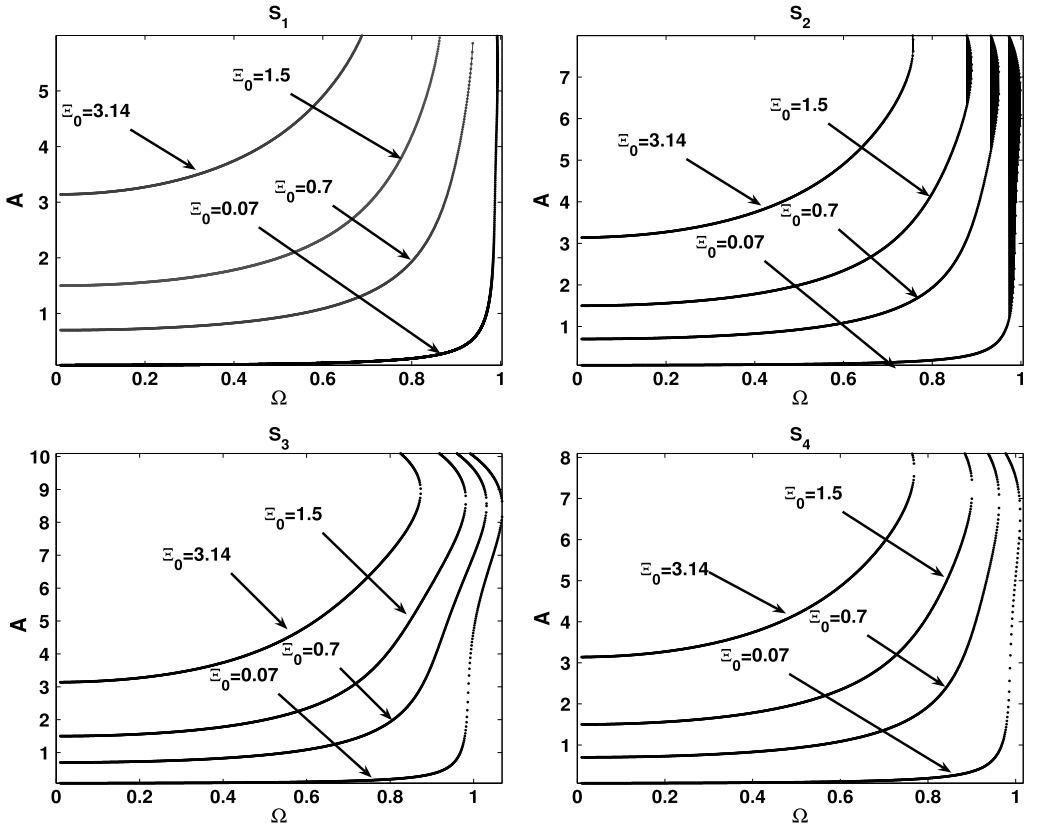

Fig. 3. Effects of the amplitude Ξ_0 on the amplitude A versus the frequency Ω of the deterministic force. The parameters S_i are the same as in Table 1, and the nonlinear damping reads $\mu = 0.01$.

the instantaneous amplitude $A(t)$ and phase $\varphi(t)$ are given by the following Langevin equations [42,3]:

$$\begin{aligned}\frac{\mathrm{d}A}{\mathrm{d}t} &= \frac{\mu A}{128}[64 - 16A^2 + 8\alpha A^4 - 5\beta A^6] + \frac{D}{2A(1+\tau^2)} - \frac{\mu \Xi_0}{2w}\sin\psi - \eta_1(t)\\ \frac{\mathrm{d}\varphi}{\mathrm{d}t} &= \nu - \frac{\mu \Xi_0}{2Aw}\cos(\psi) + \eta_2(t).\end{aligned} \tag{17}$$

Here, ψ is a constant that depends on the initial conditions [43], $\eta_1(t)$ and $\eta_2(t)$ represent independent normalized Wiener processes. The potential V exists if the following condition holds [44]

$$\frac{\partial P_1}{\partial y_2} - \frac{\partial P_2}{\partial y_1} \simeq 2\nu \tag{18}$$

where

$$P_1 = -\frac{\partial V}{\partial y_1}, \qquad P_2 = -\frac{\partial V}{\partial y_2}$$

and the two variables $y_1(t) = A\sin(\psi)$ and $y_2(t) = A\cos(\psi)$ in the plane $(x, \dot{x})$ rotate with the frequency of the drive, w. Following Ref. [44], the effective Langevin equation (17) amounts to a Brownian motion of a particle in a double well potential. The effective pseudo-potential $U(A, \psi)$ is given by

$$U(A,\psi) = -\frac{\mu}{128}\left[32A^2 - 4A^4 + \frac{4}{3}\alpha A^6 - \frac{5}{8}\beta A^8\right] + \frac{\mu \Xi_0}{2w}A\sin(\psi) - \frac{D\ln(A)}{2(1+\tau^2)}. \tag{19}$$

When one considers the driven modified BvdP equation (4) with sinusoidal drive but without stochastic perturbation, Eq. (19) reduces to:

$$U(A,\psi) = -\frac{\mu}{128}\left[32A^2 - 4A^4 + \frac{4}{3}\alpha A^6 - \frac{5}{8}\beta A^8\right] + \frac{\mu \Xi_0}{2w}A\sin(\psi). \tag{20}$$

Table 2
Domain of existence of stable limit cycles. The parameters S_i are the same as in Table 1. All data refer to the case $\mu = 0.01$.

$S_i = (\alpha, \beta)$	Phase ψ	Domain of Ξ_0	Number of solutions
$S_1 = (0.114; 0.003)$	$\psi = -\frac{\pi}{2}$	$\Xi_0 \in [0; 1.31]$	3 solutions
	$\psi = +\frac{\pi}{2}$	$\Xi_0 \in [0; 1.14]$	4 solutions
$S_2 = (0.1; 0.002)$	$\psi = -\frac{\pi}{2}$	$\Xi_0 \in [0; 0.791]$	3 solutions
	$\psi = +\frac{\pi}{2}$	$\Xi_0 \in [0; 1.802]$	2 solutions
$S_3 = (0.12; 0.0016)$	$\psi = -\frac{\pi}{2}$	$\Xi_0 \in [0; 0.806]$	3 solutions
	$\psi = +\frac{\pi}{2}$	$\Xi_0 \in [0; 0.397]$	2 solutions
$S_4 = (0.12; 0.0024)$	$\psi = -\frac{\pi}{2}$	$\Xi_0 \in [0; 0.806]$	3 solutions
	$\psi = +\frac{\pi}{2}$	$\Xi_0 \in [0; 0.613]$	2 solutions

This potential depends on the excitation amplitude Ξ_0. Stationary oscillations are obtained if $\partial U/\partial\psi = 0$ and $\partial U/\partial A = 0$, and the corresponding equations for the amplitude and phase read

$$\cos(\psi) = 0 \tag{21a}$$

$$A\left\{\frac{5}{64}\beta A^6 - \frac{\alpha}{8}A^4 + \frac{1}{4}A^2 - 1 + \frac{\Xi_0}{Aw}\sin(\psi)\right\} = 0. \tag{21b}$$

In the new variables (A, ψ), the parameters μ, α and β are fixed in the region of birhythmicity of Fig. 2. A sufficient condition for the limit-cycle oscillation to be a stationary stochastic process is that the parameter ψ assumes to take the values $\psi = \pm\pi/2$, as can be seen from Eq. (21a).

The resulting amplitudes are plotted in Fig. 4 as a function of the amplitude Ξ_0 for different values of $S_i = (\alpha, \beta)$. Fig. 4(a) shows the variation of the amplitude A versus the amplitude Ξ_0 for $\psi = -\pi/2$ and the sets of parameters S_i. It appears that the bi-rhythmic behavior persists and strongly depends on the amplitude Ξ_0. When Ξ_0 is too large, a transition between three limit cycle solutions and one limit cycle solution appears, for the set of parameters S_1. For low drive amplitude Ξ_0 where two stable amplitudes and one unstable amplitude are observed (Fig. 4), the limit amplitude excitation for which one still obtains three amplitudes is reported in Table 2. Fig. 4(b) also shows the amplitude of the oscillations as a function of the deterministic drive, but with $\psi = \pi/2$. One finds either four solutions (S_1, two stable and two unstable solutions), or two solutions (S_2, S_3, S_4, one stable and one unstable). For large Ξ_0 values, the limit cycles quench and the possibility of different solutions disappears.

To analyze the effects of correlation time τ on the amplitude–response $A(\Xi_0)$, we consider again stationary oscillations from the pseudo-potential defined in Eq. (19) to derive the resulting amplitude as a function of the noise amplitude D and of the correlation time τ. This is shown in Fig. 5 where there appears a sudden jump: The amplitude–response shows multi-limit-solutions for low Ξ_0 and single limit-cycle when the amplitude Ξ_0 increases. The amplitude at which the jump occurs decreases when the correlation time τ increases.

The above analysis of Eq. (17) and of the pseudo-potential U given by Eq. (20), reveals that the system shows a birhythmic behavior only for $\psi = -\pi/2$, that is the value used in this paper. Having fixed the relative phase ψ, Eq. (17) gives the behavior of the pseudo-potential $U(A, \psi)$ upon the amplitude of correlated noise D, the amplitude of the deterministic force, Ξ_0, and the correlation time τ. In Fig. 6 we plot the pseudo-potential as a function of the amplitude A for the sets of parameters S_i and different values of the sinusoidal drive amplitude Ξ_0. For the case S_1 (equal frequencies for the two attractors) a moderate value of the drive amplitude, up to $\Xi_0 = 0.3$, there is not a drastic change, for the two wells remain. However the almost symmetric potential corresponding to $\Xi_0 = 0$ becomes asymmetric for the higher value of the applied drive. Also for the case S_2 (equal frequencies for the two attractors) and a moderate value of the drive amplitude, up to $\Xi_0 = 0.6$, there is not a drastic change, for the two wells remain, and the asymmetry is not removed by the drive. For the case S_3 (markedly different frequencies for the two attractors) a strong value of the drive amplitude, up to $\Xi_0 = 2\pi$, one of the orbits (the inner one) becomes unstable. Therefore, one concludes that the external drive can induce a drastic change, for the birhythmicity disappears. Finally, for the case S_4 (markedly unequal frequencies for the two attractors), even for a strong value of the drive amplitude, up to $\Xi_0 = 1.2$, there is not a drastic change, for the two wells remain. In conclusion of this part, it appears in the calculations of Fig. 6 that the effect of the periodic strength is to alter the pseudo-potential, but it does not always lead to the disappearance of one of the minima, hence the system can remain, or not, birhythmic, depending on the particular choice of the parameters.

Fig. 7 shows the effect of noise correlation time τ at a fixed (small) drive amplitude $\Xi_0 = 0.07$. In this case we note that when the two frequencies are about equal, Fig. 7(a), the correlation time τ has a significant effect on the pseudopotential and in this figure, we see that the birhythmic disappears to the proportion and as the drive amplitude Ξ_0 increases. Instead, when the two frequencies are different, Fig. 7(b), the correlation time has little effect on the shape of the pseudo-potential.

In Fig. 8, we report the influence of the amplitude Ξ_0 of the deterministic force and the correlation time τ on the stability map shown in Fig. 2. Fig. 8(a) shows the effects of the amplitude Ξ_0; one finds that the domain of the multi-limit-cycle decreases when Ξ_0 increases. Instead in Fig. 8(b) the birhythmic region increases with the increase of the correlation time τ.

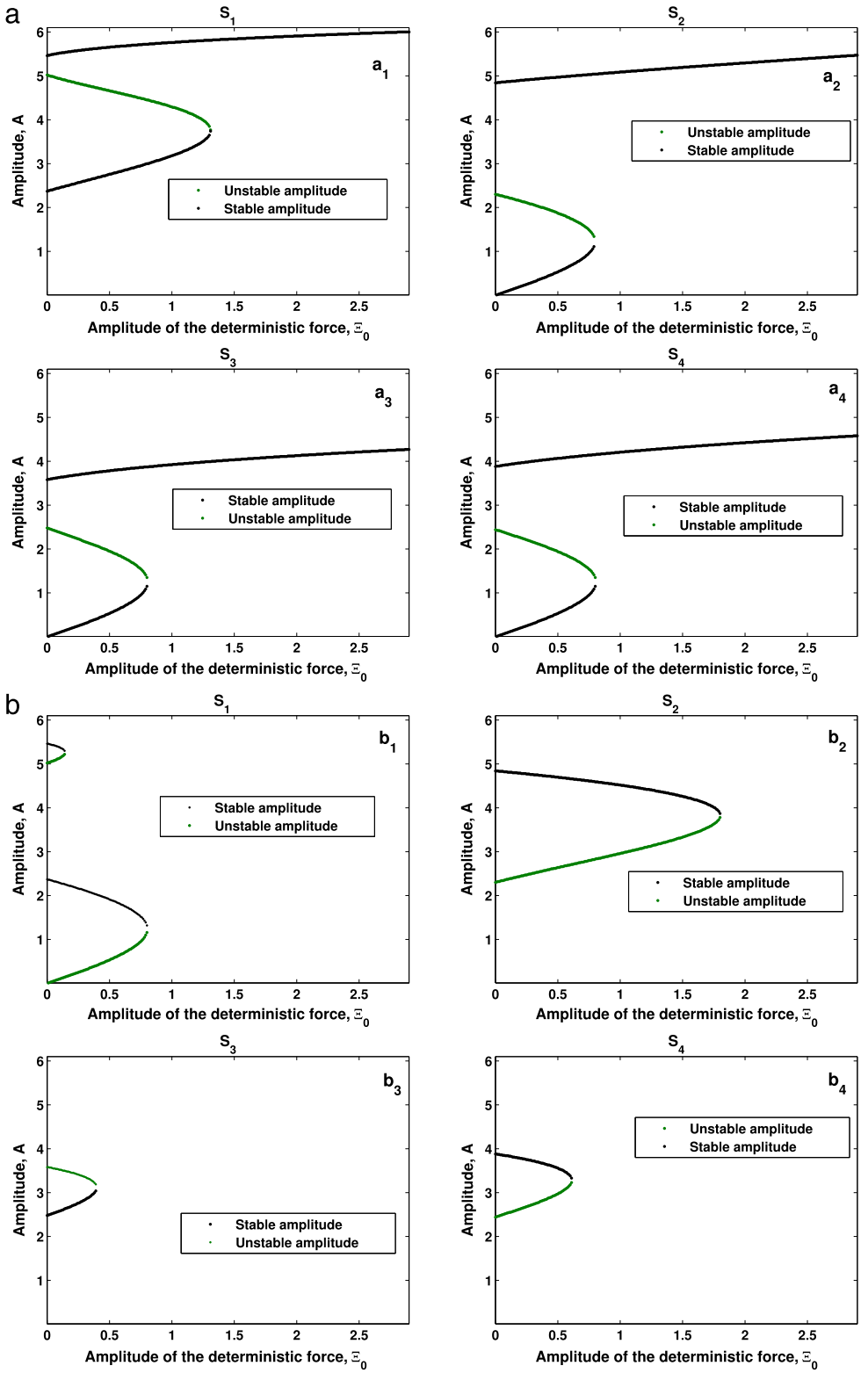

Fig. 4. Variation of the amplitude A versus the amplitude Ξ_0 of the driving force for (a) $\psi = -\frac{\pi}{2}$ and (b) $\psi = \frac{\pi}{2}$. The parameters S_i are the same as in Table 1.

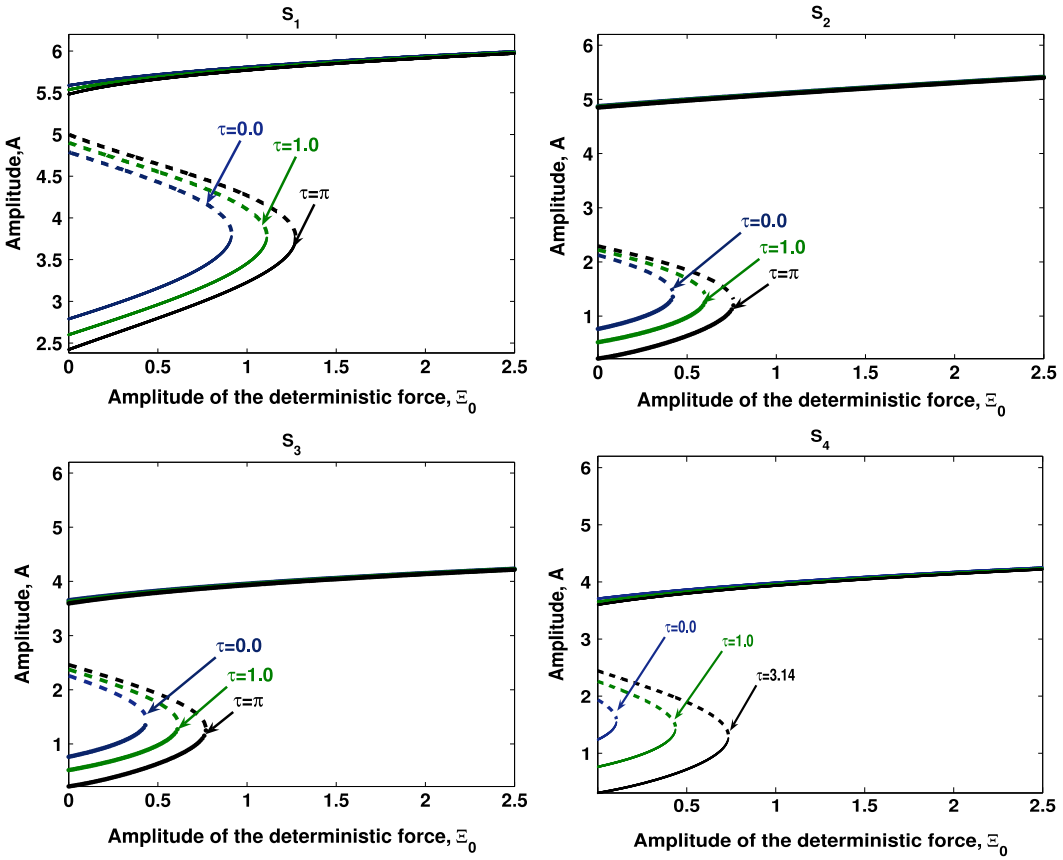

Fig. 5. Effect of the noise correlation time τ on the amplitude–response curves with $D = 0.5$, $\mu = 0.01$. The symbols S_i denote the selected points of Table 1.

Generally, the region of existence of three limit cycles, a condition for birhythmicity, decreases with the increase of the amplitude of deterministic excitation, see Fig. 8(a), and increases when the correlation time increases, see Fig. 8(b). It is also interesting to notice that when the correlation time matches the period of the forcing term ($\tau \simeq 2\pi/\Omega$) we do not observe any special features connected with this time matching. Finally in Fig. 9, we represent the bifurcation diagram for the system parameter plane (Ξ_0, τ). The domain of the existence of three limit cycles disappears when Ξ_0 increases and increases when τ increases. The same effects are observed for all parameters S_i.

4. Fokker–Planck equation of the averaged orbit probability distribution

The analytic results on the deterministic system are based on the approximated cycle given by Eq. (16), while the pseudopotential introduced in Section 3 through the relation equation (17), is only an indirect measure of the stability of the orbits if the noise intensity is assumed to be small. To be more detailed about the actual behavior of the system we retrieve in this section other characteristics that are more promptly connected with the experimental behavior, as can be retrieved for instance from circuits as that of Fig. 1.

4.1. Fokker–Planck equation

In the Langevin equation (17), dA does not depend on ψ; thus, we can develop a probability density of the amplitude A (see Ref. [16] for details). This probability is governed by Fokker–Planck–Kolmogorov equation:

$$\frac{\partial P}{\partial t} = \left[\frac{\mu A}{128}(64 - 16A^2 + 8\alpha A^4 - 5\beta A^6) + \frac{D}{2A(1+\tau^2)} - \frac{\mu \Xi_0}{2w}\sin(\psi)\right]P + \frac{D}{1+\tau^2}\frac{\partial^2 P}{\partial A^2}. \tag{22}$$

The probability distribution of the radius A (averaged over a period $2\pi/w$) is promptly obtained from the stationary solution of Eq. (22):

$$P(A) = N(1+\tau^2)A\exp\left[\mu\frac{1+\tau^2}{D}\left(\frac{1}{2}A^2 - \frac{1}{16}A^4 + \frac{\alpha}{48}A^6 - \frac{5\beta}{512}A^8 - \frac{\Xi_0}{\omega}A\sin(\psi)\right)\right]. \tag{23}$$

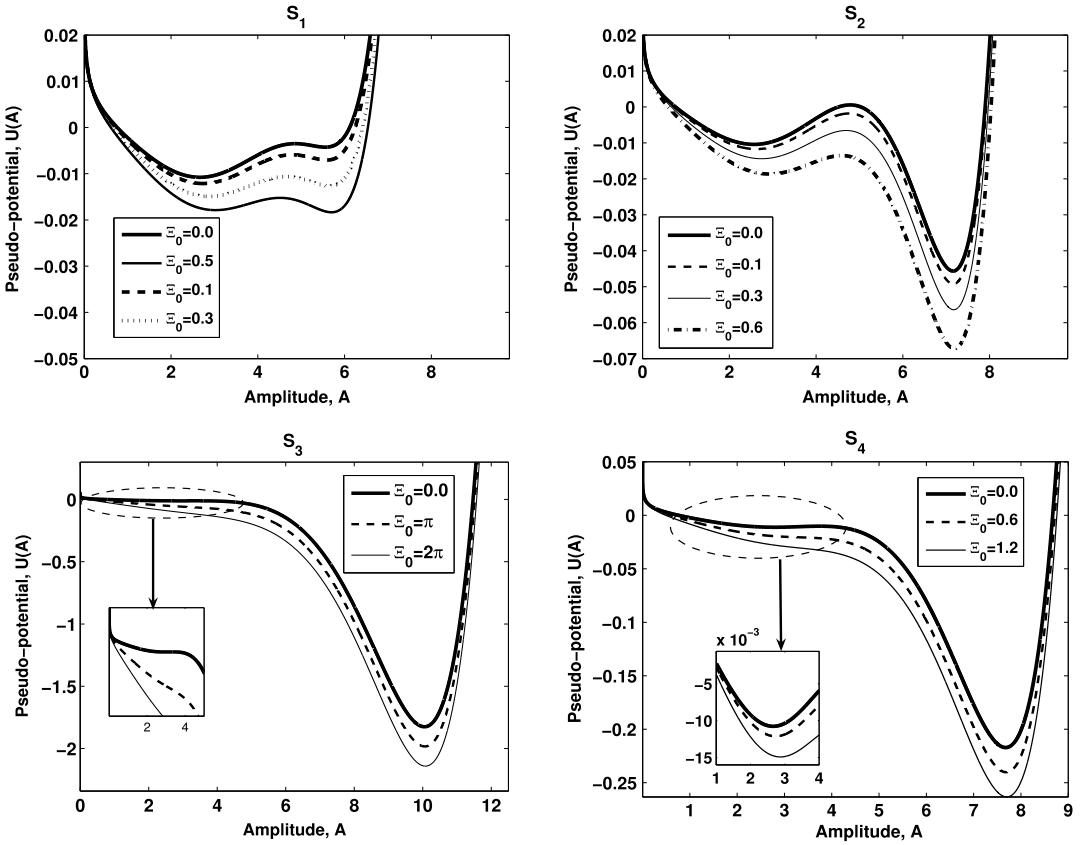

Fig. 6. Effect of the amplitude of deterministic force Ξ_0 on the potential U versus the oscillations amplitude A as per Eq. (17) with the set of parameters S_i of Table 1. The frequencies of the two attractors are identical for $i = 1, 2$ and different for $i = 3, 4$. The other parameters read $\tau = 0.01$, $D = 0.01$.

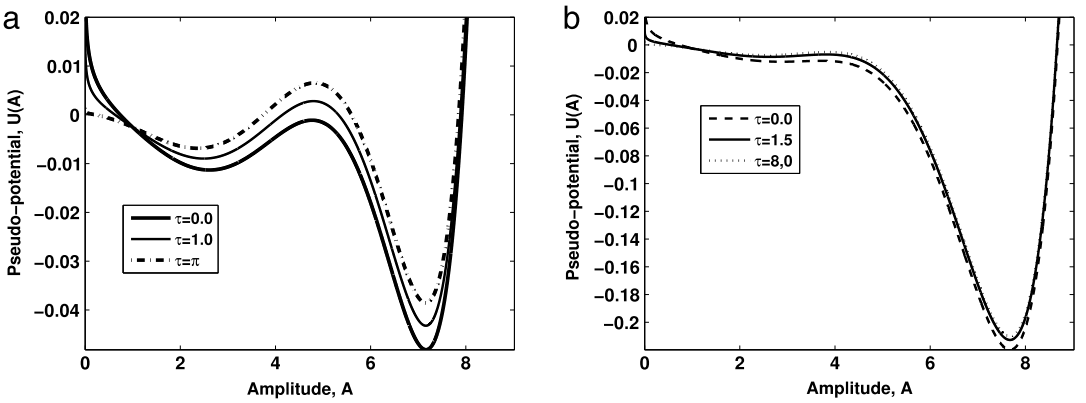

Fig. 7. Effect of correlation time τ on the potential U versus the oscillations amplitude A as per Eq. (17). The parameters S_1 (a) and S_4 (b) refer to the cases when the frequencies of two attractors are identical and different, respectively (see Table 1). The other parameters read $\Xi_0 = 0.07$, $D = 0.01$.

Here N is the normalized constant. It may be noted that the above solution has earlier been obtained by Stratonovich for the original van der Pol system [45]. Before proceeding further in our analysis, it should be noted that the peaks of the probability distribution can be located using the following equation:

$$\frac{dP}{dA} = 0 \Rightarrow A^2 - \frac{1}{4}A^4 + \frac{\alpha}{8}A^6 - \frac{5\beta}{64}A^8 - \frac{\Xi_0}{\omega}A\sin(\psi) + \frac{D}{\mu(1+\tau^2)} = 0. \tag{24}$$

For $D = 0$ and $\Xi_0 = 0$ the amplitude (24) coincides with the deterministic amplitude equation (9), also derived in Ref. [34] and of the pseudopotential (19).

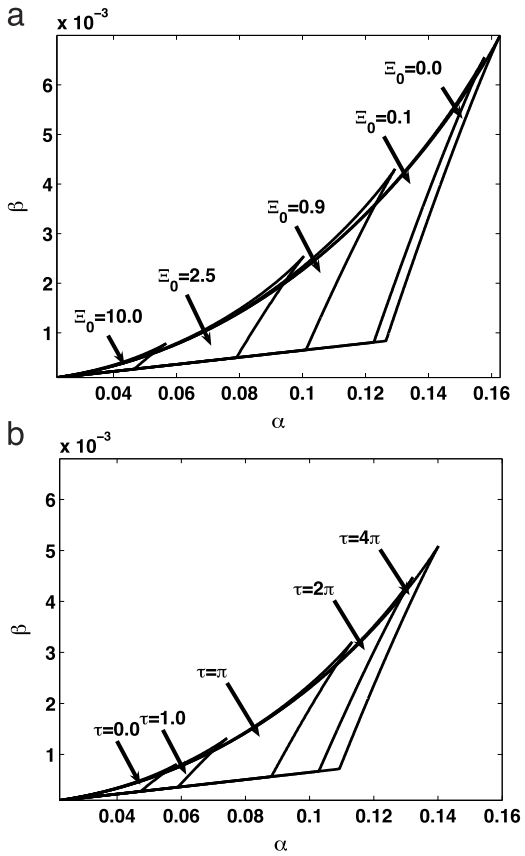

Fig. 8. (a) Bifurcation diagram in the domain (α, β) for different values of amplitude Ξ_0 with $\mu = 0.01$, $D = 0.002$, $\tau = 0.2$. (b) Bifurcation diagram in the domain (α, β) for different values of correlation time τ with $\mu = 0.01$, $D = 0.5$, $\Xi_0 = 0.5$.

One concludes that the probability distribution (23), as derived from the FPK equation (22), reproduces the analytical properties of the deterministic system and predicts the effects of the correlation time, driving strength, and noise intensity on the birhythmic properties of BvdP system of Fig. 1.

4.2. Transition rates

In Section 3 we have discussed the presence of more than one stable orbit. Random fluctuations and an applied periodic term in the case of multiple attractors (two stable and one unstable, in our case) can induce a transition between two stable attractor. Thus, the metastable states are characterized by a rate, precisely the frequency at which the attractor is left by the representative coordinate. Let $R_{1,3}$, the residence times, be the quantities which measure the relative stabilities pertaining to the attractors 1 and 3:

$$R_1 = \int_0^{A_2} P(A)\mathrm{d}A, \tag{25a}$$

$$R_3 = \int_{A_2}^{\infty} P(A)\mathrm{d}A. \tag{25b}$$

The transition from the two attractors over the potential barrier $\Delta U_{1,3}$ can be described by the Langevin type equation (17) by the well known Kramers' escape rate $r^k_{1,3}$ (with the appropriated rescaled noise intensity $\tilde{D}$ to account for the correlation time):

$$r^k_{1,3} = \frac{\sqrt{U''(A_{1,3}) \mid U''(A_2) \mid}}{2\pi} \exp\left(-\frac{\Delta U_{1,3}}{\tilde{D}}\right) \tag{26}$$

in the limit $\tilde{D} \ll \Delta U_{1,3}$. The rate decreases inversely proportional to the noise amplitude D and for long periods [46].

The inverse of the Kramers escape rate, $T_i = 1/r^k_i$ is the average escape time from one well to another. (Thus, T_1 corresponds to the average transition time of the system from attractor with limit-cycle amplitude A_1 to attractor with limit-cycle amplitude A_3, and T_3 corresponds to the reverse case.)

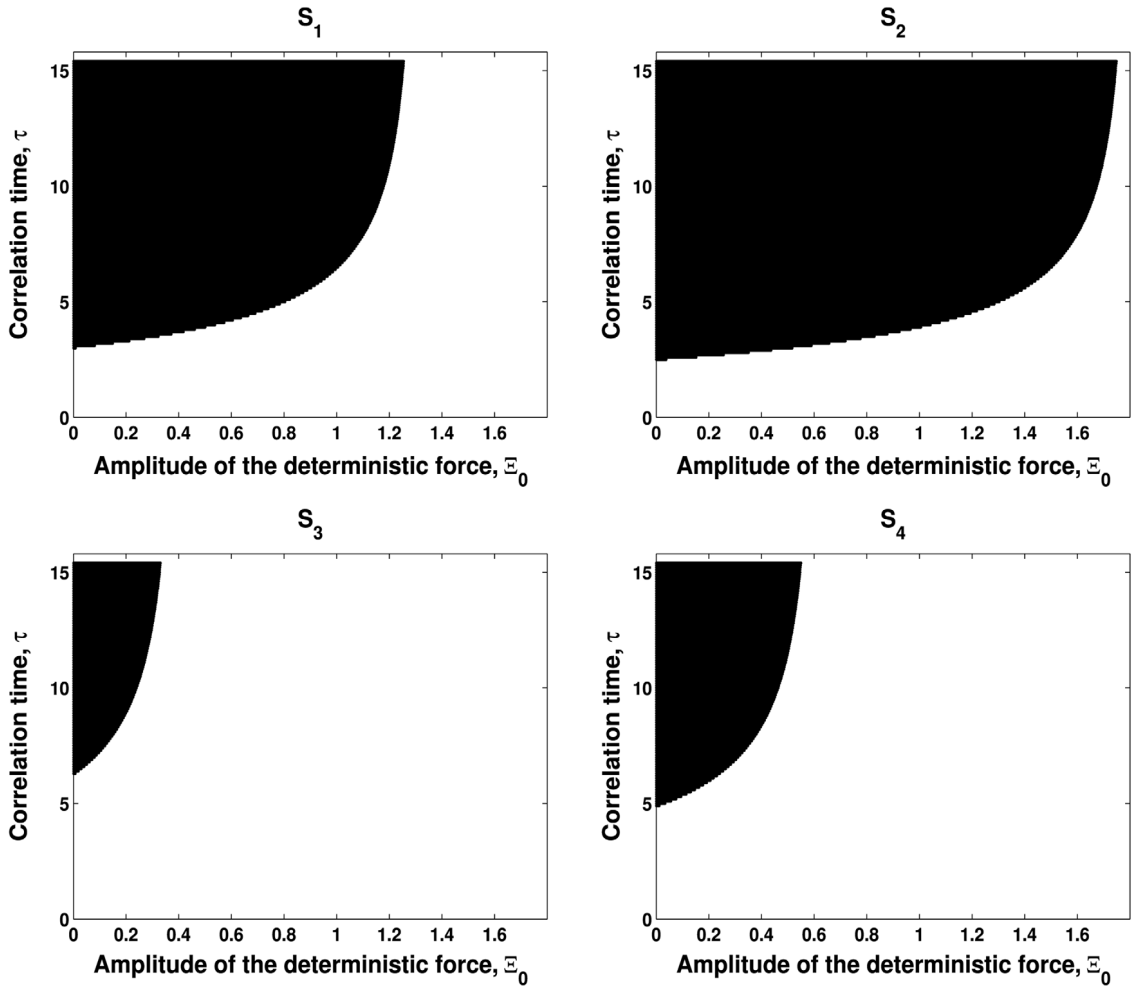

Fig. 9. Stochastic P-bifurcation diagram of the system in the parameter plane (Ξ_0, τ). The black region represents the parameter region where two stable orbits and one unstable orbit coexist. Parameters of system are $\mu = 0.01$, $D = 0.5$ and S_i $(i = 1, 2, 3, 4)$, see Table 1.

The quantities T_i are related to the probability to find the system in the surroundings of one or the other of the attractors (24) by the relation:

$$R_i = \frac{T_i}{T_1 + T_3} = \frac{1/r_i^k}{1/r_1^k + 1/r_3^k}. \tag{27}$$

This preamble is instrumental to numerical verification of the analysis of Section 3. In fact the quantities R_i are both numerically accessible through direct simulations of the full model equation (4) (or equivalently, through experimental investigation of the circuit of Fig. 1), and analytically predicted by Eq. (19) through Eqs. (26) and (27). Such control is the subject of Section 5.

5. Algorithm for colored noise and numerical results

In this section we put under scrutiny the analytical results obtained so far with numerical simulations of the model equation (4).

5.1. Numerical algorithm for colored noise

To check the validity of the approximations behind the analytic treatment that has led to the probability density function equation (22), we have performed numerical simulation of the Langevin dynamic equation (4) with a numerical algorithm of the stochastic Euler type [16,47]. Although there are several methods and algorithms to solve stochastic differential equations [48], as the implicit midpoint rule with *Heun* and *Leapfrog* methods or faster numerical algorithms such as the

stochastic version of the *Runge–Kutta* methods and a quasisymplectic algorithm [48,49], we have opted for the simpler Euler method, that we have found fast enough to be employed for the present purpose. The starting point is the *Box–Muller* algorithm [47] to generate exponentially correlated colored noise $\eta_{\Delta t}$ from the Gaussian white noise and two random numbers a and b which are uniformly distributed on the unit interval [0, 1]. To simulate the exponentially correlated colored noise, Eqs. (8) are replaced with the following equations [25]:

$$\dot{x} = u, \tag{28a}$$

$$\dot{u} = \mu(1 - x^2 + \alpha x^4 - \beta x^6)u - x + \eta, \tag{28b}$$

$$\dot{\eta} = -\lambda\eta + \lambda g_w, \tag{28c}$$

where g_w is a Gaussian white noise:

$$\langle g_w(t)\rangle = 0$$

$$\langle g_w(t)g_w(t')\rangle = 2D\delta(t - t'). \tag{29}$$

Combining Eqs. (28c) and (29) one gets an exponentially correlated colored noise η. To numerically solve Eqs. (28), we use the Box–Muller algorithm [47] to generate a Gaussian white noise g_w from two random numbers a and b, which are uniformly distributed on the unit interval, through the formula $g_w = [-4D\Delta t \ln(a)]^{1/2}\cos(2\pi b)$. Here, Δt denotes the integration step size. Consequently:

$$\begin{aligned}\eta(t + \Delta t) &= \mathrm{e}^{-\lambda\Delta t}\eta(t) + \lambda\int_0^{t+\Delta t} \mathrm{d}s\, \mathrm{e}^{-\lambda(t+\Delta t-s)}g_w(s)\\ &= \mathrm{e}^{-\lambda\Delta t}\eta(t) + h(t, \Delta t).\end{aligned} \tag{30}$$

Now, $h(t, \Delta t)$ is Gaussian (because g_w is) and has zero mean (because g_w does). Therefore its properties are determined by the second moment

$$\langle h^2(t, \Delta t)\rangle = D\lambda(1 - \mathrm{e}^{-2\lambda\Delta t}). \tag{31}$$

Also the averaging entailed in Eq. (6b) is performed with a similar scheme applied to the initial distribution of $\eta(0)$. Thus, to start the simulation, an initial value for η is needed and it is obtained as per Eq. (6b).

Numerical quasi-random algorithms can be used to realize both Eqs. (28) and g_w in Eq. (5), thus Eqs. (28) are treated as three coupled equations in the variables, η, x and u. This yields the Euler version of the integration of Eq. (4):

$$m, n = \text{random numbers} \tag{32a}$$

$$\eta = [-2D\lambda \ln(m)]^{1/2}\cos(2\pi n) \tag{32b}$$

$$a, b = \text{random numbers}, \tag{32c}$$

$$h = [-2D\lambda(1 - \exp(-2\lambda\Delta t))\ln(a)]^{1/2}\cos(2\pi b), \tag{32d}$$

$$x_{|t+\Delta t} = x + u\Delta t, \tag{32e}$$

$$u_{|t+\Delta t} = u + \left[\mu(1 - x^2 + \alpha x^4 - \beta x^6)u - x + \eta\right]\Delta t, \tag{32f}$$

$$\eta_{|t+\Delta t} = \exp(-\lambda\Delta t)\,\eta + h. \tag{32g}$$

The above equations have been integrated halving the step size until consistent results are obtained (the problem is particularly delicate in the proximity of an absorbing barrier [49]). Furthermore, the procedure has been calibrated with a standard activation barrier to retrieve the Kramers escape rate, as modified by the correlation time τ [50]. In the end, we have found that a step size $\Delta t = 0.0001$ is generally appropriated, but in few cases an even smaller step has been necessary. Moreover, we have averaged the results over 200 realizations, that ensure convergence within few percents.

5.2. Numerical results

We collect here the simulations of Eq. (4) with numerical simulations of Eqs. (32) to confirm the analytical results of previous sections. We begin by investigating the low noise behavior to check that the pseudo-potential approximation is valid, as shown in Fig. 10. The numerical simulations have been performed retrieving the escape rate, analogous to Eq. (26), from numerical simulations of Eq. (4). This prediction of the theoretical analysis, as summarized by Eq. (19), is confirmed in Fig. 10, where we plot numerical (dashed lines) and analytical (solid lines) energy barrier ΔU_1 and ΔU_3 as a function of the periodic signal intensity Ξ_0 for different values of the correlation time τ. In the figure, black lines and green lines denote ΔU_1 and ΔU_3, respectively, for the parameters a_i and b_i the combination correlation time and periodic signal intensity on the stability of the two attractors [51]. We systematically observe the same behavior for all parameters: the inner barrier increases when the amplitude of the drive increases, while the other barrier decreases. The effect of the colored noise source is not qualitatively altered by the periodic driving force, for the effective Fokker–Planck approximation at small colored noise is similar to the homogeneous case [52–54]. We also note that even in the presence of additive colored noise (as well as of

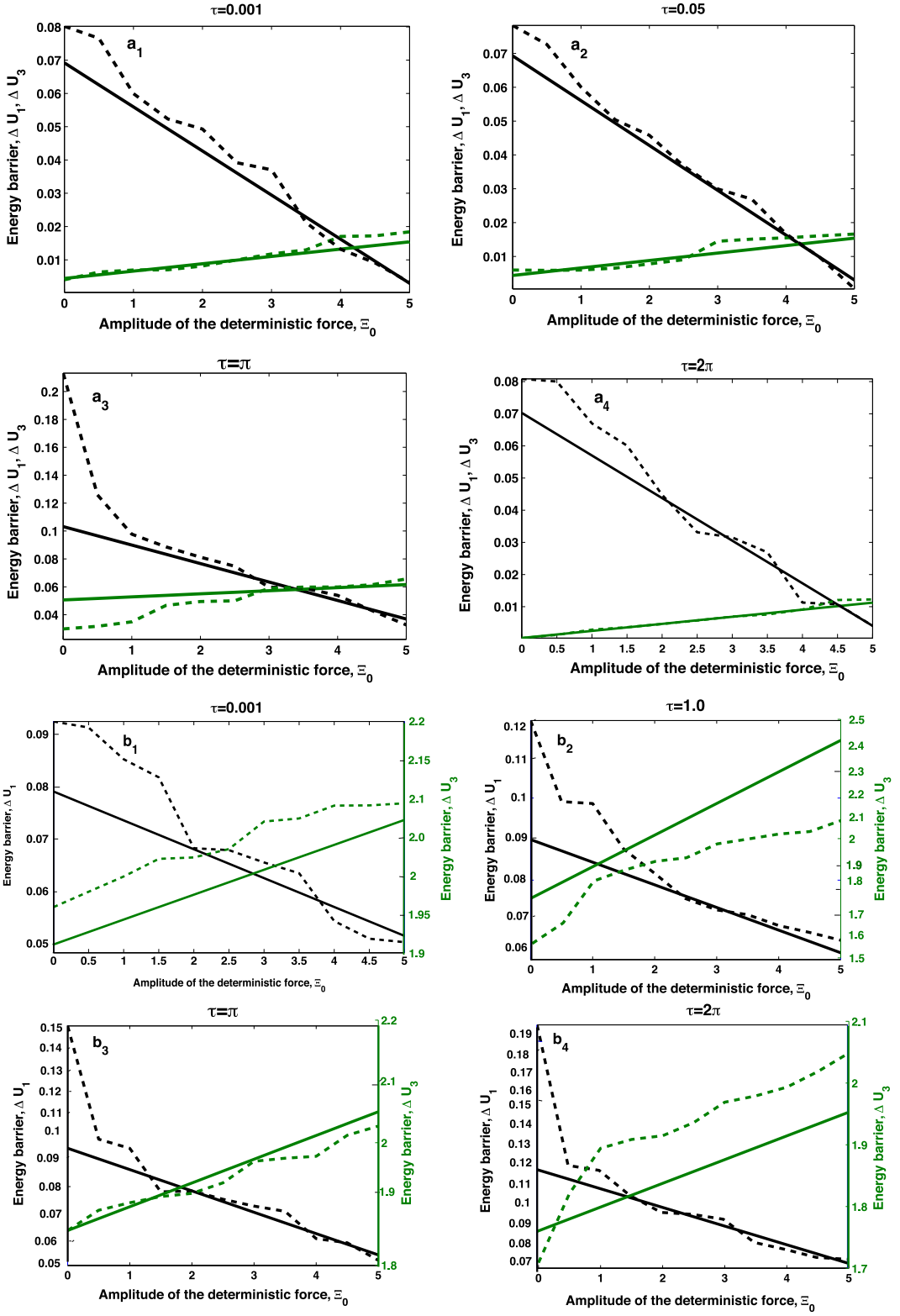

Fig. 10. Comparison of analytical (as per Eq. (19), solid lines) and numerical (as per Eq. (4), dashed lines) energy barriers for different values of the correlation time τ and as a function of the amplitude of the sinusoidal drive Ξ. Increasing light gray lines denote the inner effective energy barrier ΔU_1, while the decreasing dark lines denote the outer effective energy barrier ΔU_3. The parameters of the system are: a_i corresponding to $\alpha = 0.114$; $\beta = 0.003$, b_i's correspond to $\alpha = 0.12$; $\beta = 0.0024$. In all panels $\mu = 0.01$.

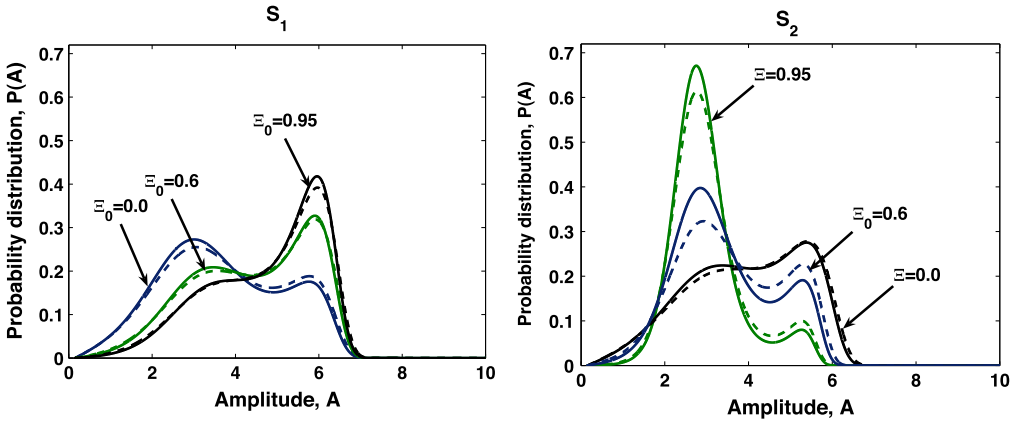

Fig. 11. Probability distributions, analytic (as per Eq. (23), solid lines) and numerical (as per Eq. (4), dashed lines) for different values of the amplitude of deterministic force Ξ_0 versus the amplitude A when the frequencies of both attractors are identical i.e. $\Omega_1 \cong \Omega_3 \cong 1$. The parameters of the system correspond to the sets S_i of Table 1 with $D = 0.03$ and $\tau = 0.05$.

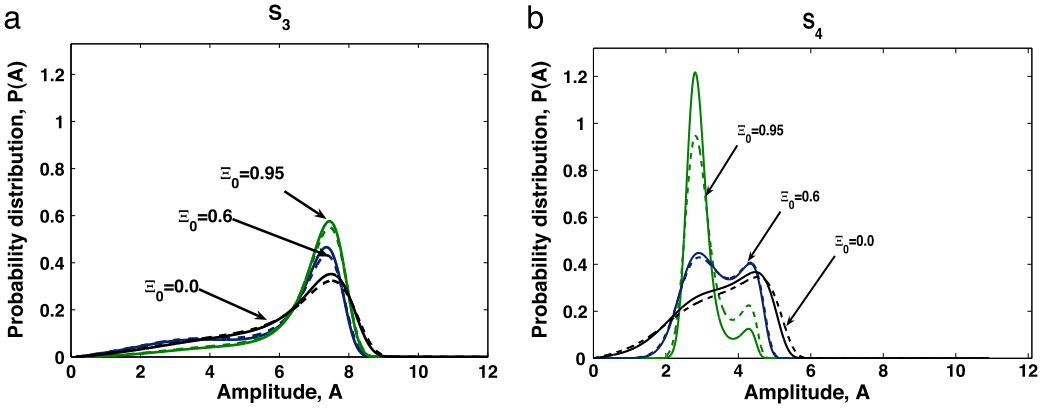

Fig. 12. Probability distributions, analytic (as per Eq. (23), solid lines) and numerical (as per Eq. (4), dashed lines) when the frequencies of the attractors are different i.e. $\Omega_1 \neq \Omega_3$. The parameters of the system correspond to the sets S_i of Table 1 with $D = 0.06$ and $\tau = 0.009$.

a deterministic force) there exists only one invariant set of trajectories in the phase space, characterized with a defined stationary probability density and can produce the disappearance of the dynamical bifurcations which are connected with the change of the stability of the invariant set (as for white noise [18]).

In Figs. 11 and 12, we compare the numerical results with the analytical predictions, Eq. (23), of the behavior of the probability distribution function $P(A, t)$ for fixed values of correlation time noise intensity and for several values of the excitation Ξ_0 (solid lines denote the analytical result and dashed lines denote numerical results). The frequencies of both attractors are about equal in Fig. 11, and markedly different in Fig. 12. It appears that the system is more likely found at two distances from the origin, the essential feature of birhythmicity. The stationary solutions $P(A)$ undergo a transition from bimodal to unimodal distribution by increasing the excitation Ξ_0. We also observe that the probability distribution changes with a small variation of the parameters α and β [11,12,16]. In general, for the set of parameters S_i, the probability distribution is asymmetric, and one can localize the probability function around a single orbit that is overwhelming more stable. In Fig. 12 for S_3 we observe a qualitative change increasing the amplitude Ξ_0: one of the minima disappears and so does the possibility to observe a birhythmic behavior. Such qualitative transformation of the probability distribution $P(A)$ in the presence of correlated noise and deterministic force is denoted as a P-bifurcation. Stochastic P-bifurcations corresponding to the appearance and disappearance of one of the maxima of the amplitude probability distribution $P(A)$ characterize the borders of the bimodal region. Thus, we conclude that noise can drastically modify the dynamics of a deterministic system. The combination of noise, driving force and nonlinear dynamics can also produce times series that are easily mistakable for chaotic deterministic system: this is especially true in the vicinity of bifurcation points, where both noise and driving force have the greatest influence. Nevertheless, the numerical distributions $P(A)$ are qualitatively similar to those obtained for the oscillator described by Eq. (4) in the quasi harmonic approach (so, the transformation of the distribution low connected with P-bifurcation results in a change of the power spectrum [55]). It is important to note that the agreement between numerical and analytical results is fairly good and in all the configurations. This is somehow surprising, for the phase amplitude approximation is not appropriated when the frequencies of the attractors are different.

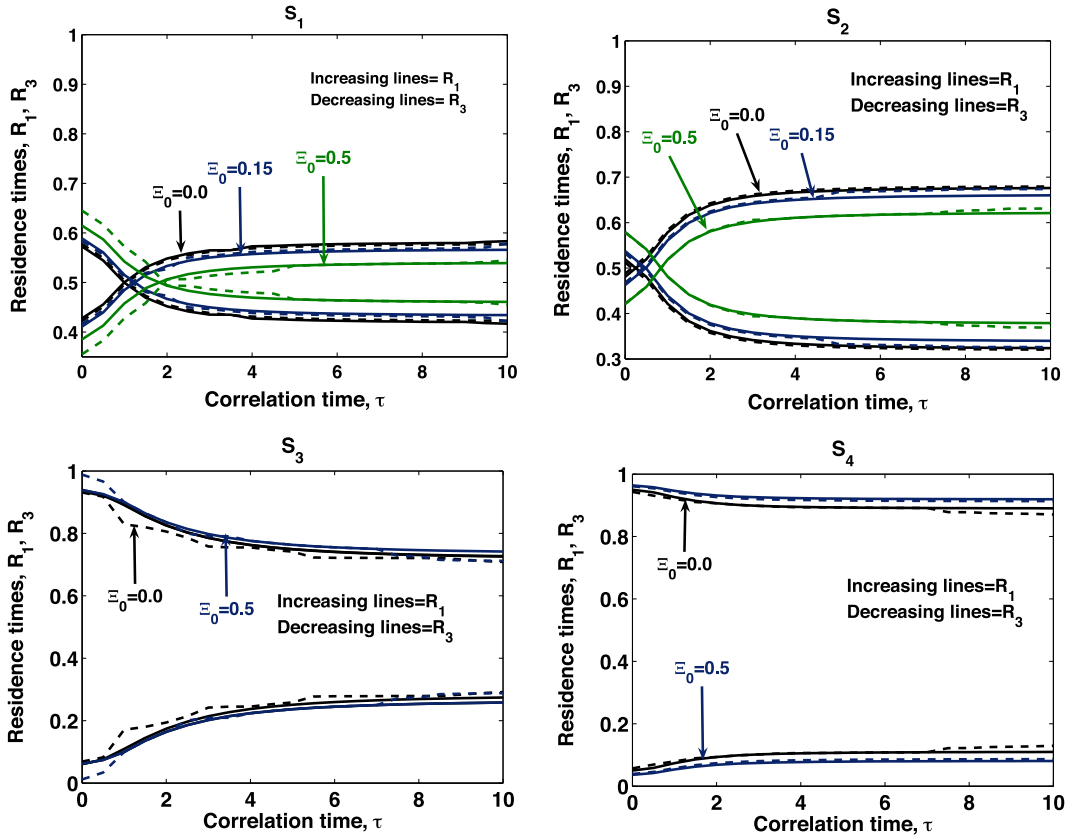

Fig. 13. Residence times, analytic (as per Eqs. (26) and (27), solid lines) and numerical (as per Eq. (4), dashed lines) as a function of the correlation time τ for different values of excitation Ξ_0 corresponding to the parameter of the system (Table 1) when the frequencies are about equal $\Omega_1 \cong \Omega_3 \cong 1$ (S_1, S_2), or the frequencies are different, $\Omega_1 \neq \Omega_3$ (S_3, S_4). All data correspond to $D = 0.05$ and $\mu = 0.01$.

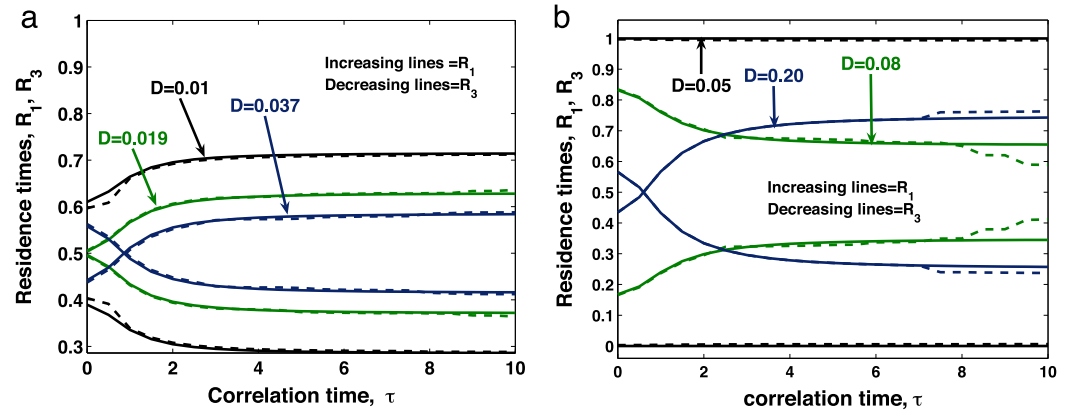

Fig. 14. Residence times, analytic (as per Eqs. (26) and (27), solid lines) and numerical (as per Eq. (4), dashed lines) as a function of the correlation time τ for different value of noise intensity D corresponding to: (a) the case where the frequencies are about equal $\Omega_1 \cong \Omega_3 \cong 1(\alpha = 0.114; \beta = 003)$ or (b) the case where the frequencies are different $\Omega_1 \neq \Omega_3$ ($\alpha = 0.12$; $\beta = 0.0024$). All data correspond to $\Xi_0 = 0.15$ and $\mu = 0.01$.

The residence times $R_{1,3}$, Eq. (25), as a function of correlation time (for different values of noise intensity D and of the drive amplitude Ξ_0) are plotted in Figs. 13 and 14; dashed lines represent the numerical results and solid lines the analytical results. As for the unperturbed birhythmic system [9,11], we confirm that also for the forced BvdP the transition between the two opposite cases where one attractor is overwhelming dominant (i.e., change of two order of magnitudes of the relative resident times) occurs within a very narrow change of the control parameters α and β [11,12,16].

To summarize the effect of correlation time τ and of the forcing term Ξ_0, we focus on the point where the two residence times are equal, i.e. when the two lines in Figs. 13 and 14 cross each other and $T_1 \simeq T_3$. Some relevant data are shown

Table 3
Coordinates $(\Xi_0; \tau)$ for the symmetric case $R_1 \simeq R_3$. The parameters S_i are the same as in Table 1. All data refer to the case $D = 0.05$.

$S_i = (\alpha, \beta)$	(τ, Ξ_0)	$R_1 = R_3$ analytical	$R_1 = R_3$numerical
$S_1 = (0.114; 0.003)$	(1.0; 0.0)	0.4995	0.4997
	(1.03; 0.15)	0.5110	0.5109
	(2.07; 0.5)	0.4937	0.4937
$S_2 = (0.1; 0.002)$	(0.17; 0.0)	0.5123	0.5111
	(0.51; 0.15)	0.4941	0.4944
	(1.0; 0.5)	0.4813	0.4813

in Table 3, where we also compare numerical and analytical results. We note that there is good approximation between analytical and numerical results. The particular point where the residence times are equal is rare when the frequencies of the oscillations are different (see S_3 and S_4), and in the simulated cases only appears for the highest values of the noise intensity ($D = 0.20$ in Fig. 14).

6. Conclusion

We have systematically investigated a bistable – more precisely a birhythmic – system, a variation of the van der Pol model that can be realized with electronic circuits (Fig. 1) and reproduces some features of oscillations in biological systems. We have found the response to the combined effect of correlation noise and a deterministic sinusoidal drive taking advantage of stochastic averaging to reduce the modified van der Pol equation (4) to an asymmetric bistable system driven by colored correlated noise. This technique has enabled us to retrieve an approximated Fokker–Planck equation that can be analytically managed. The reduction has allowed to determine various properties of the birhythmic system: the range of existence of the birhythmic region, as modified by the external drive amplitude and the correlation time, the dependence of the amplitude of the oscillations as a function of the drive amplitude and frequency, the existence of stochastic P-bifurcations. Moreover, we have been able to characterize the stability of the solutions with a pseudo-potential (or quasi-potential), that describes the low noise limit of the stability properties. The analytical tools show that the system undergoes sharp transitions at critical values of correlation time, noise intensity and excitation amplitude.

We have then turned our attention to the numerical verification of the analytical properties with numerical simulations. In some selected points we have confirmed that the analytical results are adequate to describe the original system. In particular, we have verified the behavior of the probability distribution function and of the energy barriers, as derived from the stochastic averaging. Thus, we conclude that the analytical approach proposed yields reasonably good approximation and that the numerical results follow the same qualitative behavior of the analytical estimates.

We conclude that correlated noise and sinusoidal forcing can be analytically handled for this birhythmic variant of the van der Pol oscillator, which is somehow surprising for the contemporary presence of two limit cycles.

Acknowledgments

GF acknowledges financial support from “Programma regionale per lo sviluppo innovativo delle filiere Manifatturiere strategiche della Campania” Filiera WISCH, Progetto2: Ricerca di tecnologie innovative digitali per lo sviluppo sistemistico di computer, circuiti elettronici e piattaforme inerziali ad elevate prestazioni ad uso avionico.

References

[1] D. Gonze, M. Kaufman, Theory of non-linear dynamical systems, Master en Bioinformatique et Modélisation, 2012.
[2] F. Kaiser, Coherent Excitations in Biological Systems: Specific Effects in Externally Driven Self- Sustained Oscillating Biophysical Systems, Springer-Verlag, Berlin, Heidelberg, 1983.
[3] F. Kaiser, Radio Sci. 17 (1981) 17S.
[4] H.G. Enjieu Kadji, J.B. Chabi Orou, R. Yamapi, P. Woafo, Chaos Solitons Fractals 32 (2007) 862.
[5] G.Qingyu Qun Wang, Z. Lu, L. Jun, W. Jichang, Chem. Phys. Lett. 439 (2007) 327.
[6] M.E. Jewett, D.B. Forger, R.E. Kronauer, J. Biol. RHythms 14 (1999) 493.
[7] N. Geva-Zatorsky, N. Rosenfeld, S. Itzkovitz, R. Milo, A. Sigal, E. Dekel, T. Yarnitzky, Y. Liron, P. Polak, G. Lahav, U. Alon, Mol. Syst. Biol. 2 (2006) 2006.0033.
[8] M. Laurent, J. Deschatrette, C.M. Wolfrom, PLoS ONE 5 (2010) e9346. http://dx.doi.org/10.1371/journal.pone.0009346.
[9] R. Yamapi, G. Filatrella, M.A. Aziz-Aloui, Chaos 20 (2010) 013114.
[10] P. Ghosh, S. Sen, S. Riaz, D.S. Ray, Phys. Rev. E 83 (2011) 036205.
[11] R. Yamapi, G. Filatrella, M.A. Aziz-Alaoui, A. Cerdeira Hilda, Chaos 22 (2012) 0431141-9.
[12] A. Cheage Chamgoue, R. Yamapi, P. Woafo, Nonlinear Dynam. 73 (2013) 2157.
[13] L. Fuhr, M. Abreu, P. Pett, A. Relógio, Comput. Struct. Biotechnol. J. 13 (2015) 417.
[14] I.S. Proskurkin, A.I. Lavrova, V.K. Vanag, Chaos 25 (2015) 064601.
[15] S. Hartzell, M.S. Bartlett, L. Virgin, A. Porporato, J. Theoret. Biol. 368 (2015) 83.
[16] R. Mbakob Yonkeu, R. Yamapi, G. Filatrella, C. Tchawoua, Commun. Nonlinear Sci. Numer. Simul. 33 (2016) 70.
[17] H. Horsthemke, R. Lefever, Noise Induced Transitions, springer-Verlag, Berlin, 1984.
[18] L. Arnold, Random Dynamical System, Springer, Berlin, 2003.
[19] R. Yang, A. Song, Internat. J. Modern Phys. B 22 (30) (2008) 5365.
[20] P. Addesso, G. Filatrella, V. Pierro, Phys. Rev. E 85 (2012) 016708.

[21] R.L. Stratonovich, Topics on the Theory of Random Noise, Vol. 1, Gordon and Breach, New York, 1963, Vol. 7, 1967.
[22] P.S. Landa, P.V.E. McClintock, Phys. Rep. 323 (2000) 1.
[23] S. Zhu, A.W. Yu, R. Roy, Phys. Rev. A 34 (1986) 4333.
[24] H. Busch, M.-Th. Hütt, F. Kaiser, Phys. Rev. E 64 (2001) 021105.
[25] R.F. Fox, I.R. Gatland, R. Roy, G. Vemuri, Phys. Rev. A 38 (1998) 5938.
[26] Z. Zhihong, Y. Shaopu, Comput. Electr. Eng. 41 (2015) 1.
[27] P. Hanggi, P. Talkner, M. Borkovec, Rev. Modern Phys. 62 (1990) 251.
[28] R. Yamapi, H.G. Enjieu Kadji, G. Filatrella, Nonlinear Dynam. 61 (2010) 275.
[29] D.G. Luchinsky, P.V.E. McClintock, M.I. Dykman, Rep. Progr. Phys. 61 (1998) 889.
[30] F. Marchesoni, E. Menichella-Saetta, M. Pochini, S. Santucci, Phys. Lett. A 130 (1988) 467.
[31] Chun Li, Zheng-Lin Jia, Dong-Cheng Mei, Front. Phys. (2015) 95.
[32] P. Grigolini, Chem. Phys. Lett. 47 (1977) 483.
[33] M. Ferrario, P. Grigolini, J. Math. Phys. 20 (1979) 2567.
[34] A. Cheage Chamgoue, R. Yamapi, P. Woafo, Eur. Phys. J. Plus 127 (2012) 59.
[35] R.H. Rand, Lecture Notes on Nonlinear Vibrations, Version 52, 2005.
[36] V.S. Anishchenko, T.E. Vadivasova, J. Commun. Technol. Electron. 47 (2002) 117.
[37] M.I. Dykman, M.A. Krivoglaz, Sov. Phys.—JETP 50 (1978) 30.
[38] R. Graham, T. Tél, Phys. Rev. A 31 (1985) 1109.
[39] R.L. Kautz, Phys. Lett. A 125 (1987) 315;
R.L Kautz, J. Appl. Phys. 62 (1987) 198;
R.L. Kautz, Phys. Rev. A 38 (1998) 2066.
[40] P. Hanggi, P. Riseborough, J. Am. Phys, V. 51 (1983) 347.
[41] Y. Xu, R. Gu, H. Zhang, W. Xu, J. Duan, Phys. Rev. E 83 (2011) 0562151-7.
[42] Peng Wang, Alexandre M. Tartakovsky, Daniel M. Takovsky, Phys. Rev. Lett. 110 (2013) 140602.
[43] R.N. Iyengar, P.K. Dash, Trans. ASME J. Appl. Mech. 45 (1978) 393.
[44] C.S. Manohar, R.N. Iyengar, Int. J. Non-Linear Mech. 26 (1991) 679.
[45] R.L. Stratonovich, Topics in the Theory of Random Noise, Vol. II, Gordon and Breach, New York, 1967.
[46] D. Goulding, S. Melnik, D. Curtin, T. Piwonski, J. Houlihan, J.P. Gleeson, G. Huyet, Phys. Rev. E 76 (2007) 031128.
[47] D.E. Knuth, The Art of Computer Programming, Vol. 2, Addison-Wesley, Reading MA, 1969.
[48] R. Mannella, Internat. J. Modern Phys. C 13 (2002) 1177.
[49] R. Mannella, Phys. Rev. E 69 (2004) 0411071.
[50] P. Hanggi, P. Jung, Adv. Chem. Phys. 89 (1995) 239.
[51] A. Fiasconaro, B. Spagnolo, Phys. Rev. E 80 (2009) 0411101-6.
[52] F. Moss, P.V.E. McClintock (Eds.), Noise in Nonlinear Dynamic Systems, Vol.1, Cambridge university press, 1989.
[53] J.M. Sancho, M. San Miguel, S.L. Katz, J.D. Gunton, Phys. Rev. A 26 (1982) 1589.
[54] P. Hanggi, F. Marchesoni, P. Grigolini, Phys. B 56 (1984) 333.
[55] A. Zakharova, T. Vadivasiva, V. Anishchenko, A. Koseska, J. Kurths, Phys. Rev. E 81 (2010) 011106.